The Aeronautical Journal (2025), **129**, pp. 651–670
doi:10.1017/aer.2024.68

ROYAL AERONAUTICAL SOCIETY

RESEARCH ARTICLE

Intelligent sliding mode fault-tolerant control for aircraft engines with actuator dynamics and faults based on adaptive dynamic programming

L.F. Xiao[1], Y.S. Tan[1], Y.B Du[2] and X.L Zhang[1]

[1]College of Energy and Power Engineering, Nanjing University of Aeronautics and Astronautics, Nanjing, China
[2]Automation Engineering, Nanjing University of Aeronautics and Astronautics, Nanjing, China
Corresponding author: L.F. Xiao; Email: lfxiao@nuaa.edu.cn

Received: 4 September 2023; **Revised:** 11 June 2024; **Accepted:** 9 July 2024

Keywords: sliding mode fault-tolerant control; adaptive dynamic programming; aircraft engine; actuator dynamics; actuator faults; Grey Wolf Optimizer

Abstract

The fault-tolerant control issue of aircraft engines with actuator dynamics and faults is investigated in this paper. By proposing a novel intelligent sliding mode fault-tolerant control (ISMFTC) method, which combines an adaptive dynamic programming (ADP) sliding surface with Grey Wolf Optimizer (GWO) for controller parameter optimisation, the goal is to achieve quality steady-state and dynamic performance in aircraft engines while maintaining strong fault-tolerance properties. Firstly, by considering not only actuator dynamics but also actuator faults, an uncertain nonlinear cascaded model of aircraft engines is developed according to characteristic of aircraft engines and their actuators. Secondly, an ADP-based sliding surface is proposed for considered aircraft engine uncertain nonlinear cascaded system. It can obtain a certain sense of optimised performance, and could be solved by ADP strategy off-line as well. Thirdly, fault-tolerant controller is obtained on the basis of sliding mode theory and adaptive fault estimation law, namely, ADP-based ISMFTC controller. Meanwhile, GWO is integrated into the investigation of ADP-based ISMFTC controller, optimised designable control parameters are obtained subsequently. Besides, robustness analysis is elaborated according to Lyapunov theory, fault estimation error is bounded and states of closed-loop system are uniformly ultimately bounded. Simulation on a twin-shaft turbofan aircraft engine, indicates the effect of proposed ADP-based ISMFTC method.

Nomenclature

A_8	nozzle throat area
e_{cH}	residual error of the NN expression
GWO	Grey Wolf Optimizer
$H(\cdot)$	Hamiltonian function
$J()$	optimal cost function
$\boldsymbol{K}_f$	learning rate matrix in adaptive law
$\boldsymbol{K}_s$	positive control gain matrix
n_h	high pressure compressor speed
n_l	low pressure compressor speed
p	number of neurons
$\mathbb{Q}(\cdot)$	positive semi-definite matrix
T_5	total temperature of low-pressure turbine
u	input vector
$\boldsymbol{u}_{fault}$	actuator fault vector
$V(t)$	Lyapunov function
$W_f b$	fuel flow

© The Author(s), 2024. Published by Cambridge University Press on behalf of Royal Aeronautical Society.

https://doi.org/10.1017/aer.2024.68 Published online by Cambridge University Press

$\boldsymbol{W}_c$	ideal NN weights
x	state vector
$\dot{x}$	state vector derivative
$\hat{x}$	state vector estimation
$\tilde{x}$	state vector error
x^*	optimal control state vector
y	output vector

Greek symbol

α	diagonal matrix
ε	unknown approximation error of this NN
$\boldsymbol{\varrho}$	external disturbance
$\boldsymbol{\eta}$	lumped uncertainty vector

1.0 Introduction

The aircraft engine provides thrust to move aircraft forward and speed to take off. Increasing demands on the performance of aircraft engines have resulted from development of science and technology in industry, which undoubtedly makes design of aircraft engine control more challenging [1–3]. The control systems in aircraft engines are implemented by many kinds of actuators. Due to high temperature, high pressure and alternating stress in aircraft engines, actuator faults are prone to inevitably appear. In the event of serious faults, the consequences would be unimaginable. Obviously, a fault-tolerant control (FTC) is especially crucial for aircraft engines.

Because of strong robustness and comparatively easy policy, sliding mode control (SMC) method and SMC-based FTC strategy have garnered significant attention from researchers in the field of science and engineering worldwide [4–10]. During design of SMC and closed-loop systems, it is important to design a sliding surface which is not susceptible to mismatch uncertainty [11, 12]. In Ref. [13], a disturbance observer was developed to estimate unmatched disturbances in the system, and the estimated disturbance is then utilised to derive sliding surface. The observer for disturbance increased sophistication and inconvenience of a controller design. According to Ref. [14], integral SMC law has two parts, one continuous and one discontinuous. By rejecting mismatched uncertainties through the continuous part of control, sliding surface became insensitive. In this process, continuous control is achieved through complex zero-sum games and online neural network training, which are not beneficial for practical use and engineering achievements. In Refs [15, 16], optimal control was utilised to design sliding surfaces, yet they were unable to obtain sliding surfaces to adapt mismatched uncertainties.

Reference [17] proposed a multi-regulation control strategy for single-input systems, with regulators in the form of sliding mode used for regulation. The design method was expounded through a detailed simulation example about thrust control of a turbofan engine. Detailed simulation examples of turbofan engine thrust control were presented to illustrate the design method. Based on an online estimation, which uses gradient adaptation law and low-pass filter, Ref. [18] proposed an adaptive SMC method for aircraft engines. Reference [19] proposed a sliding mode control method to ameliorate the fixity of aircraft engine, simulation was given based on a linear model of aircraft engine. All of Refs [17–19] did not consider the fault of actuators. In Ref. [20], based on an adaptive diagnostic observer, a novel sliding mode fault-tolerant control (SMFTC) strategy was proposed for aircraft engine systems with uncertainties and disturbances. Ref. [21] presented an intelligent FTC strategy for a more electric AC/DC hybrid electric power system for aircraft, aiming at ensuring the safety of aircraft engine and improving quality of power supply. However, both Refs [20, 21] did not take the actuator dynamics into consideration.

Adaptive dynamic programming (ADP) approach has strong relationship with optimal control [22], and ADP arithmetic has also been applied to the design of SMC in recent years. In Ref. [23], neural-network for a species of uncertain nonlinear systems via ADP was investigated, which is based on robust

https://doi.org/10.1017/aer.2024.68 Published online by Cambridge University Press

optimal control, and the uncertain nonlinear system's robust optimal controller was derived by means of adding a feedback gain to the optimal control design of nominal system. Main objective of Ref. [24] was to design a SMC methodology based on ADP, as a result, the closed-loop system with time-varying disturbances could be stable and the approximately optimal control performance of sliding mode dynamics can be promised. In Ref. [14], ADP was introduced to integral SMC for systems with mismatched disturbance, but ADP was merely employed to stabilise sliding mode dynamics instead of designing sliding surface at first hand. Reference [25] studied an FTC scheme for a species of cascade nonlinear systems based on SMC and ADP, however, actuator dynamics and control parameters optimisation were not taken into consideration.

In light of the reaching law approach being widely used in SMC to achieve satisfactory reaching mode, many intelligent optimal control algorithms are incorporated into the design of SMC for advancement of intelligent optimisation. One such example is the Grey Wolf Optimizer (GWO). As it is named, GWO simulates predatory behaviour of grey wolf [26]. Because of advantage that off-line GWO is simple to realise with high precision, GWO has been applied to many practical applications, in recent years [21, 27, 28]. It can be observed that GWO is one of the promising optimal algorithms for achieving low and similar designable parameter optimisation in SMFTC for aircraft engines.

Therefore, the purpose of this paper is to put forward an intelligent sliding mode fault-tolerant control (ISMFTC) method based on ADP, for aircraft engines with actuator dynamics and faults, together with mismatched uncertainties and parameter optimisation issues.

The primary contributions are summarised as follows.

- An uncertain nonlinear cascaded model of aircraft engines with actuator dynamics and faults is developed.
- A novel ADP-based sliding surface is designed for aircraft engines, which has good robustness to mismatched uncertainties, and chattering is well suppressed.
- An intelligent sliding mode fault-tolerant controller is proposed based on GWO, and combined with adaptive fault estimation strategy to deal with actuator faults in aircraft engines.
- Robustness analysis is given based on Lyapunov theory, including stability of sliding surface and reaching ability of sliding surface. It is demonstrated that the fault estimation error is bounded and closed-loop system states are uniformly ultimately bounded (UUB).

The structure of this remaining paper is as follows: Section 2 shows the control problem formulation of aircraft engines, including development of uncertain nonlinear cascaded model of aircraft engines with actuator dynamics and faults, and control objective of this paper. Section 3 presents the design of ADP-based intelligent SMFTC (ADP-based ISMFTC) method for aircraft engines. Both ADP-based sliding surface design and sliding mode fault-tolerant controller design are given in Subsection 3.1. Subsection 3.2 illustrates the robustness analysis, not only stability of sliding surface is proposed, but also reaching ability of sliding surface is expressed. Intelligent parameters optimisation for ADP-based SMFTC based on GWO, is considered in Subsection 3.3. Simulation on a twin-shaft turbofan aircraft engine is shown in Section 4, so that the effect of proposed ADP-based ISMFTC strategy is confirmed. Section 5 draws the conclusions of this paper.

2.0 Control problem formulation of aircraft engines

2.1 Nonlinear model of aircraft engines

Aircraft engines are characterised by their high complexities and nonlinearities, and can be described by

$$\dot{\boldsymbol{x}} = \boldsymbol{f}(\boldsymbol{x}, \boldsymbol{u}) \tag{1a}$$

$$\boldsymbol{y} = \boldsymbol{g}(\boldsymbol{x}, \boldsymbol{u}) \tag{1b}$$

https://doi.org/10.1017/aer.2024.68 Published online by Cambridge University Press

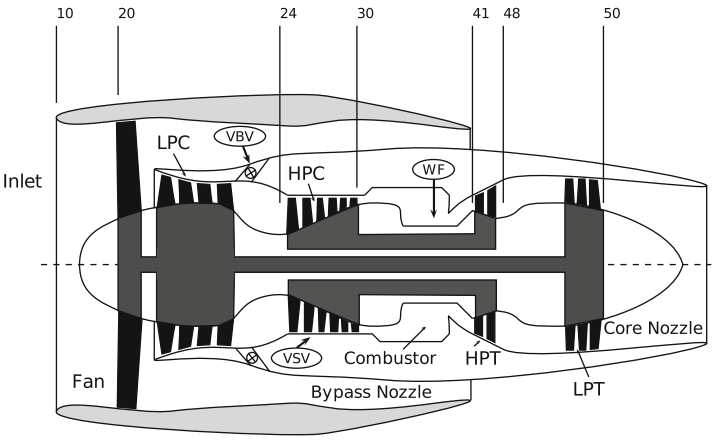


Figure 1. *General structure of aircraft engine [1].*

where $\boldsymbol{x} = [x_1, \cdots, x_n]^{\mathrm{T}} \in \mathcal{R}^n$ represents state vector, $\boldsymbol{u} = [u_1, \cdots, u_m]^{\mathrm{T}} \in \mathcal{R}^m$ represents the input vector, $\boldsymbol{y} = [y_1, \cdots, y_r]^{\mathrm{T}} \in \mathcal{R}^r$ represents the output vector. n, m, and r are the dimensions of state, input and output, respectively. $\boldsymbol{f}(\cdot)$ and $\boldsymbol{g}(\cdot)$ are nonlinear vector functions, respectively.

For a twin-shaft aircraft engine, state vector x can include low-pressure spool speed n_l and high-pressure spool speed n_h; control vector u may contain main fuel flow W_{fb}, nozzle throat area A_8; output vector y can be composed of low-pressure spool speed n_l, total temperature of low-pressure turbine T_5.

A typical general structure of twin-shaft turbofan aircraft engine is shown in Fig. 1 [1]. Fan, low-pressure compressor (LPC) and low-pressure turbine (LPT) are connected by a single shaft and thus rotate synchronously. High-pressure compressor (HPC) and high-pressure turbine (HPT) are located adjacent to the combustor and are connected by a separate shaft. Numbers are used to identify engine stations, only part of numbers are shown in Fig. 1. For example, numbers 20–24 are used to designate points between fan inlet and LPC outlet, and numbers 41–48 is used for HPT. Fuel flow (WF) is delivered by a pump, variable bleed valve (VBV) and variable stator vanes (VSV), which are the actuators utilised in this type of aircraft engine. For some aircraft engines, nozzle throat area is adjustable as well.

Hence, for a twin-shaft turbofan aircraft engine, low-pressure spool speed n_l and high-pressure spool speed n_h can be chosen as state vector $\boldsymbol{x}$; fuel flow W_{fb} and nozzle throat area A_8 may be contained in control vector $\boldsymbol{u}$; some measurable variables, such as high-pressure spool speed n_h, total temperature of low-pressure turbine T_5, can be used to compose output vector $\boldsymbol{y}$, while some calculated variables, such as thrust, compressor surge, can also be combined into output vector $\boldsymbol{y}$ [20, 21, 29].

Obviously, the dynamic model of aircraft engine in (1) is too complex, which should be avoided in designing control laws to minimise computation load and meet real-time requirements more efficiently. Therefore, linearised aircraft engine dynamic model is often utilised in controller design, particularly for prolonged operation at specific points like the rated working point or cruise point. Generally, the linearised dynamic model of (1) is given as

$$\dot{\boldsymbol{x}} = A\boldsymbol{x} + B\boldsymbol{u} \tag{2a}$$

$$\boldsymbol{y} = C\boldsymbol{x} + D\boldsymbol{u} \tag{2b}$$

In general, such a linearised model (2) is valid at steady-state operating points, primarily. To enhance the feasibility of model (2) across a wider range, one approach is to incorporate nonlinear terms [30], e.g.,

$$\dot{\boldsymbol{x}} = A\boldsymbol{x} + B\boldsymbol{u} + \boldsymbol{G}(\boldsymbol{x}) \tag{3a}$$

$$\boldsymbol{y} = C\boldsymbol{x} + D\boldsymbol{u} \tag{3b}$$

where $\boldsymbol{G}(\cdot)$ can be a very general nonlinear term.

https://doi.org/10.1017/aer.2024.68 Published online by Cambridge University Press

Through this extension, aircraft engine model becomes nonlinear again. It is hoped that nonlinear control design technique can be more convenient to carry out, compared with designing controller based on (1), while the control performance can be improved even over a large flight envelope, compared with designing controller based on (2).

Then, let $\boldsymbol{f}(\boldsymbol{x}) \triangleq A\boldsymbol{x} + G(\boldsymbol{x})$, $\boldsymbol{h}(\boldsymbol{x}, \boldsymbol{u}) \triangleq C\boldsymbol{x} + D\boldsymbol{u}$, then system (3) can be written as

$$\dot{\boldsymbol{x}} = \boldsymbol{f}(\boldsymbol{x}) + B\boldsymbol{u} \tag{4a}$$

$$\boldsymbol{y} = \boldsymbol{h}(\boldsymbol{x}, \boldsymbol{u}) \tag{4b}$$

2.2 Uncertain nonlinear cascaded model of aircraft engines with actuator dynamics and faults

Taking into account manufacturing tolerances, aging of aircraft engine, flight destabilisations, unmodeled nonlinear dynamics, and other factors, uncertainties must be accounted for in the dynamic model of aircraft engine. Thus, when considering uncertainties, corresponding uncertain model of system (4) is

$$\dot{\boldsymbol{x}} = \boldsymbol{f}(\boldsymbol{x}) + B\boldsymbol{u} + \boldsymbol{\eta} \tag{5a}$$

$$\boldsymbol{y} = \boldsymbol{h}(\boldsymbol{x}, \boldsymbol{u}) \tag{5b}$$

where $\boldsymbol{\eta}$ is the lumped uncertainty vector, including unmodelled nonlinear dynamics, parameter uncertainties and so on. For example, a description of $\boldsymbol{\eta}$ can be $\boldsymbol{\eta} = \Delta\boldsymbol{f}(\boldsymbol{x}) + \Delta B\boldsymbol{u} + \boldsymbol{\varrho}(t)$, where $\Delta\boldsymbol{f}(\boldsymbol{x})$ is the uncertainty of $\boldsymbol{f}(\boldsymbol{x})$, $\Delta B\boldsymbol{u}$ is the uncertainty of $B\boldsymbol{u}$, $\boldsymbol{\varrho}(t)$ is external disruption with respect to time.

In order to analyse the dynamic performance of actuators, first-order inertial lags are used for actuators in the design process [31], that is

$$\dot{\boldsymbol{u}} = -\boldsymbol{\alpha}^{-1}\boldsymbol{u} + \boldsymbol{\alpha}^{-1}\boldsymbol{u}_0 \tag{6}$$

where $\boldsymbol{u}_0$ is the control signal before first-order inertial lags, and $\boldsymbol{\alpha} = \mathbf{diag}\{\alpha_1, \alpha_2, ...\alpha_m\}$ is diagonal matrix. $\alpha_i > 0, (i = 1, \cdots, m)$ are time constants.

Actuators' faults should be considered, based on (5) and (6), gives

$$\dot{\boldsymbol{x}} = \boldsymbol{f}(\boldsymbol{x}) + B\boldsymbol{u} + \boldsymbol{\eta} \tag{7a}$$

$$\dot{\boldsymbol{u}} = -\boldsymbol{\alpha}^{-1}\boldsymbol{u} + \boldsymbol{\alpha}^{-1}(\boldsymbol{u}_0 + \boldsymbol{u}_{fault}) \tag{7b}$$

$$\boldsymbol{y} = \boldsymbol{h}(\boldsymbol{x}, \boldsymbol{u}) \tag{7c}$$

where $\boldsymbol{u}_{fault}$ is actuator fault vector.

Let $\bar{\boldsymbol{x}} = \left[\bar{\boldsymbol{x}}_1^{\mathrm{T}}, \bar{\boldsymbol{x}}_2^{\mathrm{T}}\right]^{\mathrm{T}} \triangleq \left[\boldsymbol{x}^{\mathrm{T}}, \boldsymbol{u}^{\mathrm{T}}\right]^{\mathrm{T}}, \boldsymbol{f}_1(\bar{\boldsymbol{x}}_1) \triangleq \boldsymbol{f}(\boldsymbol{x}), \boldsymbol{g}_1(\bar{\boldsymbol{x}}_1) \triangleq B, \boldsymbol{f}_2(\bar{\boldsymbol{x}}) \triangleq -\boldsymbol{\alpha}^{-1}\boldsymbol{u}, \boldsymbol{g}_2(\bar{\boldsymbol{x}}) \triangleq \boldsymbol{\alpha}^{-1}$, then (7) can be re-written to

$$\dot{\bar{\boldsymbol{x}}}_1 = \boldsymbol{f}_1(\bar{\boldsymbol{x}}_1) + \boldsymbol{g}_1(\bar{\boldsymbol{x}}_1)\bar{\boldsymbol{x}}_2 + \boldsymbol{\eta} \tag{8a}$$

$$\dot{\bar{\boldsymbol{x}}}_2 = \boldsymbol{f}_2(\bar{\boldsymbol{x}}) + \boldsymbol{g}_2(\bar{\boldsymbol{x}})(\boldsymbol{u}_0 + \boldsymbol{u}_{fault}) \tag{8b}$$

$$\boldsymbol{y} = \boldsymbol{h}(\bar{\boldsymbol{x}}) \tag{8c}$$

Undoubtedly, (8) shows that aircraft engine model with actuator dynamics is a species of nonlinear cascade systems [32, 33], arising mismatched uncertainties and actuator faults [34, 35]. Its structure is shown in Fig. 2.

State $\bar{\boldsymbol{x}}_2$ in subsystem (8a) is supposed virtual control [36], which can be devised based on the nominal form of system (8).

The nominal system of (8) can be written as

$$\dot{\bar{\boldsymbol{x}}}_1 = \boldsymbol{f}_1(\bar{\boldsymbol{x}}_1) + \boldsymbol{g}_1(\bar{\boldsymbol{x}}_1)\bar{\boldsymbol{x}}_2 \tag{9a}$$

$$\dot{\bar{\boldsymbol{x}}}_2 = \boldsymbol{f}_2(\bar{\boldsymbol{x}}) + \boldsymbol{g}_2(\bar{\boldsymbol{x}})\boldsymbol{u}_0 \tag{9b}$$

$$\boldsymbol{y} = \boldsymbol{h}(\bar{\boldsymbol{x}}) \tag{9c}$$

https://doi.org/10.1017/aer.2024.68 Published online by Cambridge University Press

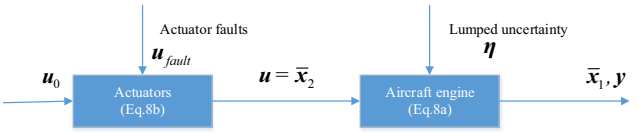


Figure 2. *Cascaded structure of aircraft engine control system with actuator dynamics.*

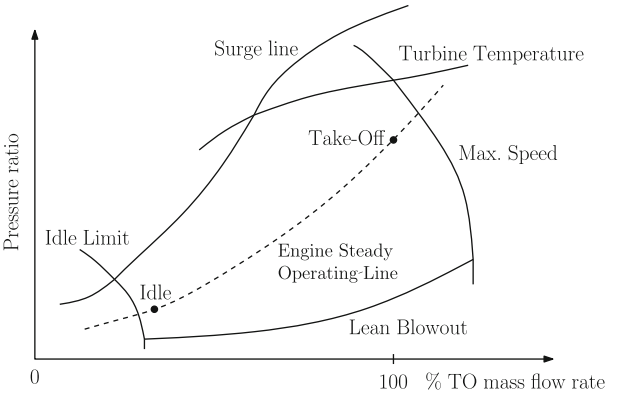


Figure 3. *Engine line and operating limits on compressor map [1].*

2.3 Control objective

The primary purpose of this paper is to design a novel sliding surface and the corresponding fault-tolerant control method. It will make the following quadratic performance indicator (10) to be minimised when the closed-loop system is approaching the designed sliding surface.

$$J = \int_t^{\infty} \mathbb{Q}(\bar{\boldsymbol{x}}_1) + \left(\bar{\boldsymbol{x}}_1^{\mathrm{T}} Q \bar{\boldsymbol{x}}_1 + \bar{\boldsymbol{x}}_2^{\mathrm{T}} R \bar{\boldsymbol{x}}_2\right) d\tau, \tag{10}$$

where $\mathbb{Q}(\cdot)$ is positive semi-definite matrix, which is associated with the lumped uncertainty, Q, R are weight matrices with appropriate dimensions. Obviously, the performance index (10) reflects the requirement on uncertainty, regulation and control law, simultaneously.

Assumption 1. *The lumped uncertainty $\boldsymbol{\eta}$ is bounded by a function $\bar{\boldsymbol{\eta}}$ with $\bar{\boldsymbol{\eta}}(0) = 0$.*

Assumption 2. *$\boldsymbol{u}_{fault}$ is an unknown bounded actuator fault vector. It can be either an unknown slowly changing fault vector or a constant bias actuator fault vector, meaning $\dot{\boldsymbol{u}}_{fault} = 0$.*

Remark 1. In (5), $\boldsymbol{\eta}$ may depend on state $\boldsymbol{x}$, since it is lumped disturbance. Commonly, it is limited to a restricted area for the operation of aircraft engine to ensure the reliability of aircraft engine [1, 37].

Figure 3 displays an aircraft engine operating line and various constraints represented on a compressor map. In Fig. 3, aircraft engine operating line represents points of compressor pressure ratio and mass flow rate obtained under steady-state conditions as the engine input changes. There are idle limit, maximum speed limit, turbine temperature limit and so on. Because speeds are selected to be state $\boldsymbol{x}$ usually, the state is bounded. Meanwhile, the control signals $\boldsymbol{u}$ in aircraft engines are limited without doubt. More detailed illustration can be found in Ref. [1]. Thus, it is suitable to assume that the lumped uncertainty $\boldsymbol{\eta}$ is bounded by a function $\bar{\boldsymbol{\eta}}$.

Remark 2. Slowly changing and constant bias actuator faults are types of common faults in aircraft engines actuators. Take faults in aircraft engines fuel pumps as an example. Among the same batch of fuel pumps, they may discharge different amounts of fuel at the same input speed, and this difference

https://doi.org/10.1017/aer.2024.68 Published online by Cambridge University Press

is a constant value. With the extension of the service time of the pump, the pump will be worn, which will affect the flow of the pump. Such a fault occurs slowly and can be regarded as slow change fault of pump.

3.0 ADP-based SMFTC design for aircraft engines

There are two common methods to reduce chattering: minimising control gain and smoothing out the control law. This paper uses an adaptive law to detect faults, reducing uncertainty and control gain. Additionally, a saturation function, or boundary layer technology, is employed in the simulation to reduce chattering.

Typically, constructing an SMC system design involves two main steps: creating a desired sliding surface and developing a suitable controller to enable the states to reach the sliding surface and maintain position on it [4, 38]. In order to ensure that the whole system is stable robustly, robustness analysis should be performed. And the robustness analysis has two parts correspondingly, one is the stability of sliding surface, the other is the reaching ability of sliding surface.

In this section, the design of ADP-based sliding surface will be given at first, then the construction of sliding mode fault-tolerant controller with adaptive law will be shown, the robustness analysis which includes analysis of both the stability of sliding surface and the reaching ability of sliding surface, will be introduced at last.

3.1 ADP-based sliding surface design

For the system (8), a ADP-based sliding mode function is designed as

$$\boldsymbol{s} = \bar{\boldsymbol{x}}_2 + \frac{1}{2} R^{-1} \boldsymbol{g}_1^T(\bar{\boldsymbol{x}}_1)(\nabla \boldsymbol{\sigma}_c(\bar{\boldsymbol{x}}_1))^{\mathrm{T}} \hat{\boldsymbol{W}}_c \tag{11}$$

where $\boldsymbol{s} = [s_1, \cdots, s_m]^{\mathrm{T}} \in \mathcal{R}^m$ is sliding mode variable for system (8), $\boldsymbol{\sigma}_c(\cdot)$ is an activation function vector of critic neural network (critic NN) in ADP, $\nabla \boldsymbol{\sigma}_c(\cdot)$ is gradient with respect to $\bar{\boldsymbol{x}}_1$ denoted as $\nabla \boldsymbol{\sigma}_c \triangleq \frac{\partial \boldsymbol{\sigma}_c}{\partial \bar{\boldsymbol{x}}_1}$, and $\hat{\boldsymbol{W}}_c$ is an estimation of ideal weight vector in ADP. The corresponding sliding surface is $\mathcal{S} = \{\bar{\boldsymbol{x}} | \boldsymbol{s}(\bar{\boldsymbol{x}}) = \boldsymbol{0}\}$.

3.2 Sliding mode fault-tolerant controller design

Let $\hat{\bar{\boldsymbol{x}}}_2^* \triangleq -\frac{1}{2} R^{-1} \boldsymbol{g}_1^T(\bar{\boldsymbol{x}}_1)(\nabla \boldsymbol{\sigma}_c(\bar{\boldsymbol{x}}_1))^T \hat{\boldsymbol{W}}_c$, then (11) turns to

$$s = \bar{\boldsymbol{x}}_2 - \hat{\bar{\boldsymbol{x}}}_2^* \tag{12}$$

hence, the derivative of sliding mode variable, i.e. $\dot{\boldsymbol{s}}$, can be written as (13) according to (11) and (8b).

$$\begin{aligned} \dot{\boldsymbol{s}} &= \dot{\bar{\boldsymbol{x}}}_2 - \dot{\hat{\bar{\boldsymbol{x}}}}_2^* \\ &= \boldsymbol{f}_2(\bar{\boldsymbol{x}}) + \boldsymbol{g}_2(\bar{\boldsymbol{x}})(\boldsymbol{u}_0 + \boldsymbol{u}_{fault}) - \dot{\hat{\bar{\boldsymbol{x}}}}_2^* \end{aligned} \tag{13}$$

The novel sliding mode fault-tolerant controller $\boldsymbol{u}_0$ with ADP-based sliding surface $\mathcal{S}$ is constructed as

$$\boldsymbol{u}_0 = \boldsymbol{g}_2^{-1}(\bar{\boldsymbol{x}}) \left(\dot{\hat{\bar{\boldsymbol{x}}}}_2^* - \boldsymbol{f}_2(\boldsymbol{x}) - \boldsymbol{K}_s \big(\mathbf{sgn}(\boldsymbol{s}) \big) \right) - \hat{\boldsymbol{u}}_{fault}, \tag{14}$$

with adaptive fault estimation law

$$\dot{\hat{\boldsymbol{u}}}_{fault} = \boldsymbol{K}_f \boldsymbol{g}_2^{\mathrm{T}}(\bar{\boldsymbol{x}}) \boldsymbol{s}, \tag{15}$$

where $\boldsymbol{K}_s, \boldsymbol{K}_f$ are positive control gain matrix (14) and learning rate matrix in adaptive law (15), respectively. $\mathbf{sgn}(s) = [\mathbf{sgn}(s_1), \cdots, \mathbf{sgn}(s_m)]^{\mathrm{T}}$, $\mathbf{sgn}(s_i), (i = 1, \cdots, m)$ are sign functions. $\hat{\boldsymbol{u}}_{fault}$ is estimation of actuator fault vector.

https://doi.org/10.1017/aer.2024.68 Published online by Cambridge University Press

3.3 Robustness analysis

3.3.1 Stability of sliding surface

When analysing stability of sliding surface $\mathcal{S}$, nominal system (9) is considered. According to (9a), $\bar{\boldsymbol{x}}_2$ can be considered as virtual control input of subsystem (10). Considering the performance index (21), optimal cost function (OCF) can be defined as

$$J^*(\bar{\boldsymbol{x}}_1) = \min_{\bar{\boldsymbol{x}}_2 \in \mathsf{A}(\Omega)} \int_t^\infty \mathbb{Q}(\bar{\boldsymbol{x}}_1) + \left(\bar{\boldsymbol{x}}_1^{\mathrm{T}} Q \bar{\boldsymbol{x}}_1 + \bar{\boldsymbol{x}}_2^{\mathrm{T}} R \bar{\boldsymbol{x}}_2\right) d\tau, \tag{16}$$

where $\mathsf{A}(\Omega)$ is admissible control set on the compact set Ω, and the Hamilton-Jacobi-Bellman (HJB) equation of this system is given as

$$0 = \min_{\bar{\boldsymbol{x}}_2 \in \mathsf{A}(\Omega)} H\left(\bar{\boldsymbol{x}}_1, \bar{\boldsymbol{x}}_2, \nabla J^*(\bar{\boldsymbol{x}}_1)\right) \tag{17}$$

where $H(\cdot)$ is the Hamiltonian function of this optimal control problem

$$\begin{aligned} H(\bar{\boldsymbol{x}}_1, \bar{\boldsymbol{x}}_2, \nabla J(\bar{\boldsymbol{x}}_1)) = {} & \mathbb{Q}(\bar{\boldsymbol{x}}_1) + (\bar{\boldsymbol{x}}_1^{\mathrm{T}} Q \bar{\boldsymbol{x}}_1 + \bar{\boldsymbol{x}}_2^{\mathrm{T}} R \bar{\boldsymbol{x}}_2) \\ & + (\nabla J(\bar{\boldsymbol{x}}_1))^{\mathrm{T}} (\boldsymbol{f}_1(\bar{\boldsymbol{x}}_1) + \boldsymbol{g}_1(\bar{\boldsymbol{x}}_1) \bar{\boldsymbol{x}}_2). \end{aligned} \tag{18}$$

with $J(0) = 0$.

Therefore, by differentiating (16) with respect to $\bar{\boldsymbol{x}}_2^*$, the optimal control policy is

$$\bar{\boldsymbol{x}}_2^* = -\frac{1}{2} R^{-1} \boldsymbol{g}_1^{\mathrm{T}}(\bar{\boldsymbol{x}}_1) \nabla J^*(\bar{\boldsymbol{x}}_1) \tag{19}$$

Considering control law (19) is unbounded, a generalised nonquadratic utility function[39] can be used to resolve problem of input constraints.

Considering (17), by substituting the optimal control policy (19) into Hamiltonian function (18), HJB Equation (17) can be given as

$$\begin{aligned} 0 &= \mathbb{Q}(\bar{\boldsymbol{x}}_1) + (\bar{\boldsymbol{x}}_1^{\mathrm{T}} Q \bar{\boldsymbol{x}}_1 + \bar{\boldsymbol{x}}_2^{*\mathrm{T}} R \bar{\boldsymbol{x}}_2^*) + (\nabla J(\bar{\boldsymbol{x}}_1))^{\mathrm{T}} (\boldsymbol{f}_1(\bar{\boldsymbol{x}}_1) + \boldsymbol{g}_1(\bar{\boldsymbol{x}}_1) \bar{\boldsymbol{x}}_2^*) \\ &= \mathbb{Q}(\bar{\boldsymbol{x}}_1) + \bar{\boldsymbol{x}}_1^{\mathrm{T}} Q \bar{\boldsymbol{x}}_1 + (\nabla J^*(\bar{\boldsymbol{x}}_1))^{\mathrm{T}} \boldsymbol{f}_1(\bar{\boldsymbol{x}}_1) \\ &\quad - \frac{1}{4} (\nabla J^*(\bar{\boldsymbol{x}}_1))^{\mathrm{T}} \boldsymbol{g}_1(\bar{\boldsymbol{x}}_1) R^{-1} \boldsymbol{g}_1^T(\bar{\boldsymbol{x}}_1) \nabla J^*(\bar{\boldsymbol{x}}_1) \end{aligned} \tag{20}$$

which means that $H(\bar{\boldsymbol{x}}_1, \bar{\boldsymbol{x}}_2^*, \nabla J^*(\bar{\boldsymbol{x}}_1)) = 0$.

The choice of $\mathbb{Q}(\bar{\boldsymbol{x}}_1)$ is important in robust stabilisation scheme. Here, $\mathbb{Q}(\bar{\boldsymbol{x}}_1)$ is specified as

$$\mathbb{Q}(\bar{\boldsymbol{x}}_1) = \tfrac{1}{8} (\nabla J^*(\bar{\boldsymbol{x}}_1))^{\mathrm{T}} \nabla J^*(\bar{\boldsymbol{x}}_1) + 2\bar{\boldsymbol{\eta}}^2 \tag{21}$$

and $\mathbb{Q}(\bar{\boldsymbol{x}}_1) \geq 0$ meets. Based on the help of this form, the following lemma showing stability of the sliding-mode dynamics of the systems (9) is derived as follows.

Lemma 1. *[25] Consider nominal subsystem (9a) and quadratic performance index (10) with the specified form of $\mathbb{Q}(\bar{\boldsymbol{x}}_1)$ (21), it is supposed that the HJB Equation (20) is a solution of $J^*(\bar{\boldsymbol{x}}_1)$. $\bar{\boldsymbol{x}}_2^*$ is given by (19), and the sliding surface defined by $\boldsymbol{s} = \bar{\boldsymbol{x}}_2 - \bar{\boldsymbol{x}}_2^* = 0$ exists. On this sliding surface, sliding-mode dynamics of this mismatched uncertain nonlinear system described by (8) is asymptotic stability.*

Proof of Lemma 1. On the basis of the Theorem 1 in [40], it is evident that the optimal control policy (19) can guarantee asymptotic stability of the uncertain nonlinear subsystem (8a). On the sliding surface, $\bar{\boldsymbol{x}}_2 = \bar{\boldsymbol{x}}_2^*(\bar{\boldsymbol{x}}_1)$ is hold and explicitly state $\bar{\boldsymbol{x}}_2$ is asymptotically convergent to the equilibrium point as well.

Because the analytical solution of the HJB Equation (20) is rather difficult to calculate, ADP with NN approximation is used in the following to find the siding surface by obtaining a numerical solution for (20).

Assumption 3. *On the compact set Ω, The ideal NN weights $\boldsymbol{W}_c$ are bounded, the NN activation functions and their gradient are bounded, the NN approximation error and its gradient are bounded, i.e., $\| \boldsymbol{W}_c \| \leq \lambda_W$, $\| \boldsymbol{\sigma}_c(\bar{\boldsymbol{x}}_1) \| \leq \lambda_\sigma$, $\| \nabla \boldsymbol{\sigma}_c(\bar{\boldsymbol{x}}_1) \| \leq \lambda_{\nabla\sigma}$, $\| \varepsilon_c(\bar{\boldsymbol{x}}_1) \| \leq \lambda_\varepsilon$, and $\| \nabla \varepsilon_c(\bar{\boldsymbol{x}}_1) \| \leq \lambda_{\nabla\varepsilon}$, where $\lambda_W, \lambda_\sigma, \lambda_{\nabla\sigma}, \lambda_\varepsilon, \lambda_{\nabla\varepsilon}$ are existing unknown boundaries.*

https://doi.org/10.1017/aer.2024.68 Published online by Cambridge University Press

Assumption 4. *For the nominal subsystem (9a) with the quadratic performance index (10) and substituting the optimal control policy (19) into the subsystem (9a), let $J_s(\bar{\boldsymbol{x}}_1)$ be a continuously differentiable function and simultaneously a Lyapunov function candidate, it is assumed that $\dot{J}_s(\bar{\boldsymbol{x}}_1)$ can be written as*

$$\dot{J}_s(\bar{\boldsymbol{x}}_1) = (\nabla J_s(\bar{\boldsymbol{x}}_1))^T \left(\boldsymbol{f}_1(\bar{\boldsymbol{x}}_1) + \boldsymbol{g}_1(\bar{\boldsymbol{x}}_1)\bar{\boldsymbol{x}}_2^*\right) < 0. \tag{22}$$

and the positive definite matrix $\Gamma \in \mathcal{R}^n$ ensures that (23) is true, where $\lambda_{min}(\Gamma)$ represents the minimal eigenvalue of the matrix Γ.

$$(\nabla J_s(\bar{\boldsymbol{x}}_1))^T \left(\boldsymbol{f}_1(\bar{\boldsymbol{x}}_1) + \boldsymbol{g}_1(\bar{\boldsymbol{x}}_1)\bar{\boldsymbol{x}}_2^*\right) = -(\nabla J_s(\bar{\boldsymbol{x}}_1))^T \Gamma \nabla J_s(\bar{\boldsymbol{x}}_1) \leq -\lambda_{min}(\Gamma) \parallel \nabla J_s(\bar{\boldsymbol{x}}_1)\|^2 \tag{23}$$

Given the sake of universal approximation property of NN, approximate $J^*(\bar{\boldsymbol{x}}_1)$ by NN with only one hidden layer can be given as

$$J^*(\bar{\boldsymbol{x}}_1) = \boldsymbol{W}_c^T \boldsymbol{\sigma}_c(\bar{\boldsymbol{x}}_1) + \varepsilon_c(\bar{\boldsymbol{x}}_1) \tag{24}$$

where $\boldsymbol{W}_c \in \mathcal{R}^p$ is the ideal weight, $\boldsymbol{\sigma}_c(\bar{\boldsymbol{x}}_1) \in \mathcal{R}^p$ is the activation function, p is the number of neurons, and $\varepsilon_c(\bar{\boldsymbol{x}}_1)$ is the unknown approximation error of this NN.

Thus, partial derivative of the OCF (24) is written as

$$\begin{aligned} \nabla J^*(\bar{\boldsymbol{x}}_1) &= \frac{\partial J^*(\bar{\boldsymbol{x}}_1)}{\partial \bar{\boldsymbol{x}}_1} \\ &= (\nabla \boldsymbol{\sigma}_c(\bar{\boldsymbol{x}}_1))^T \boldsymbol{W}_c + \nabla \varepsilon_c(\bar{\boldsymbol{x}}_1). \end{aligned} \tag{25}$$

and the optimal control policy is yielded as

$$\bar{\boldsymbol{x}}_2^* = -\frac{1}{2} R^{-1} \boldsymbol{g}_1^{\mathrm{T}}(\bar{\boldsymbol{x}})((\nabla \boldsymbol{\sigma}_c(\bar{\boldsymbol{x}}))^{\mathrm{T}} \boldsymbol{W}_c + \nabla \varepsilon_c(\bar{\boldsymbol{x}})). \tag{26}$$

Define two non-negative matrices $\mathcal{A}(\bar{\boldsymbol{x}}_1), \mathcal{B}(\bar{\boldsymbol{x}}_1)$ as

$$\begin{aligned} \mathcal{A}(\bar{\boldsymbol{x}}_1) &\triangleq \nabla \boldsymbol{\sigma}_c(\bar{\boldsymbol{x}}_1) \boldsymbol{g}_1(\bar{\boldsymbol{x}}_1) R^{-1} \boldsymbol{g}_1^{\mathrm{T}}(\bar{\boldsymbol{x}}_1)((\nabla \boldsymbol{\sigma}_c(\bar{\boldsymbol{x}}_1))^{\mathrm{T}} \\ \mathcal{B}(\bar{\boldsymbol{x}}_1) &\triangleq \nabla \boldsymbol{\sigma}_c(\bar{\boldsymbol{x}}_1)((\nabla \boldsymbol{\sigma}_c(\bar{\boldsymbol{x}}_1))^{\mathrm{T}}. \end{aligned}$$

With the quadratic performance index (10) and control policy (26) denoted by the NN, the Hamiltonian function could be given by

$$\begin{aligned} H(\bar{\boldsymbol{x}}_1, \boldsymbol{W}_c) = \bar{\boldsymbol{x}}_1^T Q \bar{\boldsymbol{x}}_1 + \boldsymbol{W}_c^{\mathrm{T}} \nabla \boldsymbol{\sigma}_c(\bar{\boldsymbol{x}}_1) \boldsymbol{f}_1(\bar{\boldsymbol{x}}_1) - \frac{1}{4} \boldsymbol{W}_c^{\mathrm{T}} \mathcal{A}(\bar{\boldsymbol{x}}_1) \boldsymbol{W}_c + 2\bar{\boldsymbol{\eta}}^2 \\ + \frac{1}{8} \boldsymbol{W}_c^{\mathrm{T}} \mathcal{B}(\bar{\boldsymbol{x}}_1) \boldsymbol{W}_c + e_{cH} = 0 \end{aligned} \tag{27}$$

where the term e_{cH} is the residual error of the NN expression.

$$\begin{aligned} e_{cH} = (\nabla \varepsilon_c(\bar{\boldsymbol{x}}_1))^T \boldsymbol{f}_1(\bar{\boldsymbol{x}}_1) - \frac{1}{2}(\nabla \varepsilon_c(\bar{\boldsymbol{x}}_1))^T \boldsymbol{g}_1(\bar{\boldsymbol{x}}_1) R^{-1} \boldsymbol{g}_1^T(\bar{\boldsymbol{x}}_1)((\nabla \boldsymbol{\sigma}_c(\bar{\boldsymbol{x}}_1))^T \boldsymbol{W}_c \\ - \frac{1}{4}(\nabla \varepsilon_c(\bar{\boldsymbol{x}}_1))^{\mathrm{T}} \boldsymbol{g}_1(\bar{\boldsymbol{x}}_1) R^{-1} \boldsymbol{g}_1^{\mathrm{T}}(\bar{\boldsymbol{x}}_1) \nabla \varepsilon_c(\bar{\boldsymbol{x}}_1) + \frac{1}{4}(\nabla \varepsilon_c(\bar{\boldsymbol{x}}_1))^{\mathrm{T}} (\nabla \boldsymbol{\sigma}_c(x_1))^{\mathrm{T}} \boldsymbol{W}_c \\ + \frac{1}{8}(\nabla \varepsilon_c(\bar{\boldsymbol{x}}_1))^{\mathrm{T}} \nabla \varepsilon_c(\bar{\boldsymbol{x}}_1) \end{aligned} \tag{28}$$

In the view that the ideal NN weights are unknown, the estimation of NN weight vector $\hat{\boldsymbol{W}}_c$ is utilised to approximate the OCF (24)

$$\hat{J}^*(\bar{\boldsymbol{x}}_1) = \hat{\boldsymbol{W}}_c^{\mathrm{T}} \boldsymbol{\sigma}_c(\bar{\boldsymbol{x}}_1) \tag{29}$$

then an approximation of the partial derivative of the OCF (24) is

$$\nabla \hat{J}^*(\bar{\boldsymbol{x}}_1) = \frac{\partial \hat{J}^*(\bar{\boldsymbol{x}}_1)}{\partial x_1} = (\nabla \boldsymbol{\sigma}_c(\bar{\boldsymbol{x}}_1))^{\mathrm{T}} \hat{\boldsymbol{W}}_c. \tag{30}$$

https://doi.org/10.1017/aer.2024.68 Published online by Cambridge University Press

the approximate optimal control policy can be expressed as

$$\hat{\bar{\boldsymbol{x}}}_2^* = -\frac{1}{2}R^{-1}\boldsymbol{g}_1^{\mathrm{T}}(\bar{\boldsymbol{x}}_1)(\nabla\boldsymbol{\sigma}_c(\bar{\boldsymbol{x}}_1))^{\mathrm{T}}\hat{\boldsymbol{W}}_c. \tag{31}$$

and the approximate Hamiltonian function is given as

$$\begin{aligned}\hat{H}(\bar{\boldsymbol{x}}_1, \boldsymbol{W}_c) = {} & \bar{\boldsymbol{x}}_1^{\mathrm{T}}Q\bar{\boldsymbol{x}}_1 + \hat{\boldsymbol{W}}_c^{\mathrm{T}}\nabla\boldsymbol{\sigma}_c(\bar{\boldsymbol{x}}_1)\boldsymbol{f}_1(\bar{\boldsymbol{x}}_1) \\ & - \frac{1}{4}\hat{\boldsymbol{W}}_c^{T}\mathcal{A}(\bar{\boldsymbol{x}}_1)\hat{\boldsymbol{W}}_c + 2\bar{\boldsymbol{\eta}}^2(\bar{\boldsymbol{x}}_1) + \frac{1}{8}\hat{\boldsymbol{W}}_c^{\mathrm{T}}\mathcal{B}(\bar{\boldsymbol{x}}_1)\hat{\boldsymbol{W}}_c\end{aligned} \tag{32}$$

Define $e_c = \hat{H}(\bar{\boldsymbol{x}}_1, \boldsymbol{W}_c) - H(\bar{\boldsymbol{x}}_1, \boldsymbol{W}_c)$, and $\tilde{\boldsymbol{W}}_c = \boldsymbol{W}_c - \hat{\boldsymbol{W}}_c$. According to (27) and (32), the e_c with respect to $\tilde{\boldsymbol{W}}_c$ is expressed as

$$\begin{aligned}e_c = {} & \hat{H}(\bar{\boldsymbol{x}}_1, \boldsymbol{W}_c) - H(\bar{\boldsymbol{x}}_1, \boldsymbol{W}_c) \\ = {} & -\tilde{\boldsymbol{W}}_c^{T}\nabla\boldsymbol{\sigma}_c(\bar{\boldsymbol{x}}_1)\boldsymbol{f}_1(\bar{\boldsymbol{x}}_1) - \frac{1}{4}\tilde{\boldsymbol{W}}_c^{\mathrm{T}}\mathcal{A}(\bar{\boldsymbol{x}}_1)\tilde{\boldsymbol{W}}_c + \frac{1}{2}\tilde{\boldsymbol{W}}_c^{\mathrm{T}}\mathcal{A}(\bar{\boldsymbol{x}}_1)\boldsymbol{W}_c \\ & + \frac{1}{8}\tilde{\boldsymbol{W}}_c^{\mathrm{T}}\mathcal{B}(\bar{\boldsymbol{x}}_1)\tilde{\boldsymbol{W}}_c - \frac{1}{4}\tilde{\boldsymbol{W}}_c^{\mathrm{T}}\mathcal{B}(\bar{\boldsymbol{x}}_1)\boldsymbol{W}_c - e_{cH}.\end{aligned} \tag{33}$$

Now, it is required to train the critic NN and to find an updated law of weights by minimising the simple cost standard $E_c = (1/2)e_c^2$.

An improved weight updated rule [40] is chosen to avoid the difficulty of obtaining a valid initial control policy.

Then, based on Assumption 4, $J_s(\bar{\boldsymbol{x}}_1)$ is given as $J_s(\bar{\boldsymbol{x}}_1) = 0.5\bar{\boldsymbol{x}}_1^{\mathrm{T}}\bar{\boldsymbol{x}}_1$, and a weight updated law of the critic NN is designed as

$$\dot{\hat{\boldsymbol{W}}}_c = -\alpha_c\left(\frac{\partial E_c}{\partial \hat{\boldsymbol{W}}_c}\right) - \alpha_s\left(\frac{\partial[(\nabla J_s(\bar{\boldsymbol{x}}_1))^{\mathrm{T}}(\boldsymbol{f}_1(\bar{\boldsymbol{x}}_1) + \boldsymbol{g}_1(\bar{\boldsymbol{x}}_1)\hat{\bar{\boldsymbol{x}}}_2^*)]}{\partial \hat{\boldsymbol{W}}_c}\right) \tag{34}$$

where $\alpha_c > 0$ and $\alpha_s > 0$ are the basic update rate of critic NN and the learning rate of the additional stabilisation term, respectively.

By substituting the optimal control strategy (31) into (34), the updated law can be expressed as

$$\dot{\hat{\boldsymbol{W}}}_c = -\alpha_c\left(\frac{\partial E_c}{\partial \hat{\boldsymbol{W}}_c}\right) + \frac{1}{2}\alpha_s\nabla\boldsymbol{\sigma}_c(\bar{\boldsymbol{x}}_1)\boldsymbol{g}_1(\bar{\boldsymbol{x}}_1)R^{-1}\boldsymbol{g}_1^{\mathrm{T}}(\bar{\boldsymbol{x}}_1)\nabla J_s(\bar{\boldsymbol{x}}_1) \tag{35}$$

Let the weight estimation error (WEE) $\tilde{\boldsymbol{W}}_c$ is $\tilde{\boldsymbol{W}}_c = \boldsymbol{W}_c - \hat{\boldsymbol{W}}_c$, due to $\boldsymbol{W}_c$ will be constant at last, $\dot{\tilde{\boldsymbol{W}}}_c = -\dot{\hat{\boldsymbol{W}}}_c$ and the dynamics of the WEE can be written as

$$\dot{\tilde{\boldsymbol{W}}}_c = \alpha_c\left(\frac{\partial E_c}{\partial \hat{\boldsymbol{W}}_c}\right) - \frac{1}{2}\alpha_s\nabla\boldsymbol{\sigma}_c(\bar{\boldsymbol{x}}_1)\boldsymbol{g}_1(\bar{\boldsymbol{x}}_1)R^{-1}\boldsymbol{g}_1^{\mathrm{T}}(\bar{\boldsymbol{x}}_1)\nabla J_s(\bar{\boldsymbol{x}}_1), \tag{36}$$

where

$$\begin{aligned}\frac{\partial E_c}{\partial \boldsymbol{W}_c} = {} & e_c\frac{\partial e_c}{\partial \boldsymbol{W}_c} \\ = {} & e_c(\nabla\sigma_c(\bar{\boldsymbol{x}}_1)\boldsymbol{f}_1(\bar{\boldsymbol{x}}_1) - \frac{1}{2}\mathcal{A}(\bar{\boldsymbol{x}}_1)\boldsymbol{W}_c + \frac{1}{4}\mathcal{B}(\bar{\boldsymbol{x}}_1)\boldsymbol{W}_c).\end{aligned}$$

https://doi.org/10.1017/aer.2024.68 Published online by Cambridge University Press

thus

$$\begin{aligned}\dot{\tilde{\boldsymbol{W}}}_c = \alpha_c \Bigg(& -\tilde{\boldsymbol{W}}_c^{\mathrm{T}} \nabla \boldsymbol{\sigma}_c(\bar{\boldsymbol{x}}_1) \boldsymbol{f}_1(\bar{\boldsymbol{x}}_1) - \frac{1}{4} \tilde{\boldsymbol{W}}_c^{\mathrm{T}} \mathcal{A}(\bar{\boldsymbol{x}}_1) \tilde{\boldsymbol{W}}_c \\ & + \frac{1}{2} \tilde{\boldsymbol{W}}_c^{\mathrm{T}} \mathcal{A}(\bar{\boldsymbol{x}}_1) \boldsymbol{W}_c + \frac{1}{8} \tilde{\boldsymbol{W}}_c^{\mathrm{T}} \mathcal{B}(\bar{\boldsymbol{x}}_1) \tilde{\boldsymbol{W}}_c - \frac{1}{4} \tilde{\boldsymbol{W}}_c^{\mathrm{T}} \mathcal{B}(\bar{\boldsymbol{x}}_1) \boldsymbol{W}_c - e_{cH}) \\ & \times \left(\nabla \boldsymbol{\sigma}_c(\bar{\boldsymbol{x}}_1) \boldsymbol{f}_1 + \frac{1}{2} \mathcal{A}(x_1) \tilde{\boldsymbol{W}}_c - \frac{1}{2} \mathcal{A}(\bar{\boldsymbol{x}}_1) \boldsymbol{W}_c - \frac{1}{4} \mathcal{B}(\bar{\boldsymbol{x}}_1) \tilde{\boldsymbol{W}}_c + \frac{1}{4} \mathcal{B}(\bar{\boldsymbol{x}}_1) \boldsymbol{W}_c \right) \\ & - \frac{1}{2} \alpha_s \nabla \boldsymbol{\sigma}_c(\bar{\boldsymbol{x}}_1) \boldsymbol{g}_1(\bar{\boldsymbol{x}}_1) R^{-1} \boldsymbol{g}_1^{\mathrm{T}}(\bar{\boldsymbol{x}}_1) \nabla J_s(\bar{\boldsymbol{x}}_1). \end{aligned} \tag{37}$$

Therefore, the following Lemma 2 illustrates the system states' property on the novel sliding surface.

Lemma 2. *In view of the nominal system described by (9) under the provided ADP-based sliding surface (11), the states of system (8) on the sliding surface and the weight error dynamics are uniformly ultimately bounded (UUB) when the sliding mode exists.*

Proof of Lemma 2. The definition of UUB can be found in [41], while according to the theorem 2 in [40], one can see that state $\bar{\boldsymbol{x}}_1$ on the sliding surface specified by (11) and dynamics of WEE are both UUB. For the sake of brevity, the proof process will not be proved repeatedly. Besides, in term of the sliding surface $\mathcal{S} = \{\bar{\boldsymbol{x}} | \boldsymbol{s}(\bar{\boldsymbol{x}}) = 0\}$, state $\bar{\mathbf{x}}_2$ of the system on this sliding surface is also UUB.

Remark 3 *It is easy to find that Assumption 4 is a general assumption, which can see details in* [42, 43]. *Besides, though the use of ADP faces the problem of the training taking too much time, it can be avoided by off-line training to make sure the real-time performance of the whole control system.*

3.3.2 Reaching ability of sliding surface

Theorem 1. *For the system described by (8) with mismatched uncertainty, actuator dynamics and faults, under the proposed control law (14), with the ADP-based sliding surface described by (11), and adaptive fault estimation law (15), the closed-loop system's states are UUB and its fault estimation error is bounded.*

Proof [Proof of Theorem 1] Select Lyapunov function as

$$V(t) = \frac{1}{2} \boldsymbol{s}^{\mathrm{T}} \boldsymbol{s} + \frac{1}{2} \tilde{\boldsymbol{u}}_{\mathrm{fault}}^{\mathrm{T}} \boldsymbol{K}_f^{-1} \tilde{\boldsymbol{u}}_{fault} \tag{38}$$

where $\tilde{u}_{fault}$ is fault estimation error, which is defined as $\tilde{\boldsymbol{u}}_{fault} = \boldsymbol{u}_{fault} - \hat{\boldsymbol{u}}_{fault}$.

One the basis of Assumption 2, along the sliding mode variable **s**, the derivative of the Lyapunov function (38) is

$$\begin{aligned} \dot{V}(t) &= \boldsymbol{s}^{\mathrm{T}} \dot{\boldsymbol{s}} - \tilde{\boldsymbol{u}}_{fault}^{\mathrm{T}} \boldsymbol{K}_f^{-1} \dot{\hat{\boldsymbol{u}}}_{fault} \\ &= \boldsymbol{s}^{\mathrm{T}} \left(\boldsymbol{f}_2(\bar{\boldsymbol{x}}) + \boldsymbol{g}_2(\bar{\boldsymbol{x}})(\boldsymbol{u}_0 + \boldsymbol{u}_{fault}) - \dot{\hat{\bar{\boldsymbol{x}}}}_2^*(\bar{\boldsymbol{x}}_1) \right) - \tilde{\boldsymbol{u}}_{fault}^{\mathrm{T}} \boldsymbol{K}_f^{-1} \dot{\hat{\boldsymbol{u}}}_{fault} \end{aligned} \tag{39}$$

Based on the control law (14) and the actuator fault compensation law (15), (39) will be expressed as

$$\begin{aligned} \dot{V}(t) &= -K_s \| \boldsymbol{s} \| + \boldsymbol{s}^{\mathrm{T}} \boldsymbol{g}_2(x) \tilde{\boldsymbol{u}}_{fault} - \tilde{\boldsymbol{u}}_{fault}^{\mathrm{T}} \boldsymbol{K}_f^{-1} \dot{\hat{\boldsymbol{u}}}_{fault} \\ &= -K_s \parallel s \parallel \\ &\leq 0. \end{aligned} \tag{40}$$

Therefore, it is clear that all states of closed-loop system are bounded. In terms of the Lyapunov theorem and Lemma 2, the sliding modes exist and the overall system exists in UUB states.

Here complete the proof.

https://doi.org/10.1017/aer.2024.68 Published online by Cambridge University Press

3.4 Intelligent parameters optimisation for ADP-based SMFTC

In this section, GWO will be employed to search the optimal control designable parameters in (14) and (15) under the multi-target performance indicators of aircraft engine are

$$J_{GWO_1} = \int_0^t \boldsymbol{x}^{\mathrm{T}} \boldsymbol{x} d\tau \tag{41a}$$

$$J_{GWO_2} = \int_0^t \boldsymbol{u}_0^{\mathrm{T}} \boldsymbol{u}_0 d\tau \tag{41b}$$

where J_{GWO_1} reflects steady-state control accuracy requirement, and J_{GWO_2} expresses the interest on input energy consumption, in view that the state deviation from the equilibrium point is expected to be as small as possible, while a minimum input energy consumption is also desired at the same time.

Generally speaking, GWO is a meta-heuristic optimisation algorithm, which is encouraged by the primary phases of grey wolf hunting.

The main mathematical equations of describing the hunting process are:

$$\begin{aligned}
&\vec{X}(t_{GWO}+1) = \vec{X}_p(t_{GWO}) - \vec{A}\vec{D} \\
&\vec{A} = 2\vec{a}\vec{r}_1 - \vec{a}, \qquad \vec{C} = 2\vec{r}_2, \qquad \vec{D} = \left|\vec{C}\vec{X}_p(t_{GWO}) - \vec{X}(t_{GWO})\right| \\
&\vec{D}_\alpha = \left|\vec{C}_1\vec{X}_\alpha - \vec{X}\right|, \qquad \vec{D}_\beta = \left|\vec{C}_2\vec{X}_\beta - \vec{X}\right|, \qquad \vec{D}_\delta = \left|\vec{C}_3\vec{X}_\beta - \vec{X}\right|, \\
&\vec{X}_1 = \vec{X}_\alpha - \vec{A}_1\vec{D}_\alpha, \qquad \vec{X}_2 = \vec{X}_\beta - \vec{A}_2\vec{D}_\beta, \qquad \vec{X}_3 = \vec{X}_\delta - \vec{A}_3\vec{D}_\delta, \\
&\vec{X}(t_{GWO}+1) = \frac{\vec{X}_1 + \vec{X}_2 + \vec{X}_3}{3}
\end{aligned} \tag{42}$$

where the current iteration is represented by t_{GWO}, the position vector of the prey and a grey wolf are given by $\vec{X}_p(t_{GWO})$ and $\vec{X}(t_{GWO})$, respectively. The subscripts $(\cdot)_\alpha$, $(\cdot)_\beta$ and $(\cdot)_\delta$ are in behalf of the $\boldsymbol{\alpha}_{GWO}$(best candidate solution), $\boldsymbol{\beta}_{GWO}$ and $\boldsymbol{\delta}_{GWO}$ grey wolves, respectively. $\vec{A}$ and $\vec{C}$ are coefficient vectors, with $\vec{a}$ is decreased from 2 to 0 in the course of iterations, linearly. $\vec{r}_1$ and $\vec{r}_2$ are stochastic vectors in the range of [0, 1]. $\vec{D}$, $\vec{X}_1$, $\vec{X}_2$ and $\vec{X}_3$ are instrumental variables.

The optimisation imitates the hunting process of grey wolves, the detailed principle of GWO can be seen in Refs [21, 44].

According to the SMC fundamental theory [38], $\boldsymbol{K}_s$ is crucial for the control performance of aircraft engine. Meanwhile, the $\boldsymbol{K}_f$ is important for the fault estimation, as shown in the control law (14) and adaptive law (15). Thus, $\boldsymbol{K}_s$ and $\boldsymbol{K}_f$ are key designable parameter matrices in ADP-based SMFTC controller for obtaining the minimum performance indexes (41).

Therefore, when GWO is applied to reach the parameter optimisation of ADP-based SMFTC for aircraft engine, the $\vec{X}(t_{GWO})$ described by (42) for each t_{GWO} can be $\vec{X} = \left[K_{s_1}, \cdots, K_{s_n}, K_{f_1}, \cdots, K_{f_n}\right]$, where $K_{s_i}, K_{f_i}, (i = 1, \cdots, n)$ are diagonal elements of $\boldsymbol{K}_s, \boldsymbol{K}_f$, respectively.

After obtaining the optimal designable parameters by GWO intelligent optimisation algorithm, the proposed ADP-based SMFTC method, is called as ADP-based intelligent SMFTC, and it is referred to as "ADP-based ISMFTC" method for short in the following.

The block diagram of the presented ADP-based ISMFTC method for aircraft engine with actuator dynamics and faults, is given in Fig. 4.

4.0 Simulation

In this section, the novel ISMFTC with the ADP-based sliding surface is applied in the uncertain nonlinear cascade model of a twin-shaft turbofan aircraft engine with actuator dynamics and faults. According

https://doi.org/10.1017/aer.2024.68 Published online by Cambridge University Press

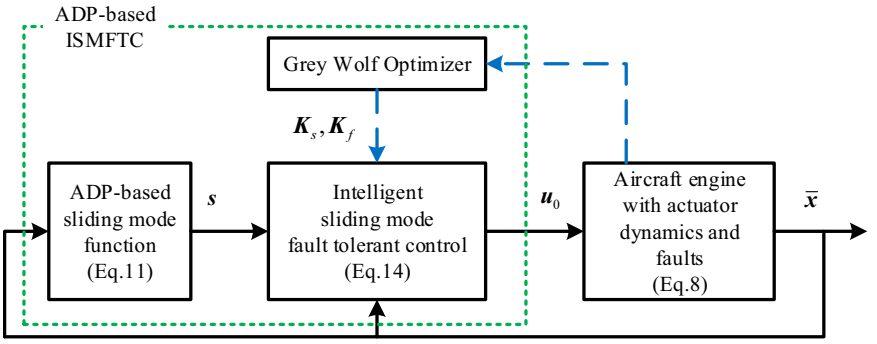


Figure 4. *The block diagram of ADP-based ISMFTC method for aircraft engine with actuator dynamics and faults.*

to (8), on the basis of [29, 30], $\boldsymbol{f}_1(\bar{\boldsymbol{x}}_1)$, B in $\boldsymbol{g}_1(\bar{\boldsymbol{x}}_1)$, $\boldsymbol{\alpha}$ in $\boldsymbol{f}_2(\bar{\boldsymbol{x}})$ and $\boldsymbol{g}_2(\bar{\boldsymbol{x}})$, lumped uncertainty vector $\boldsymbol{\eta}$, fault vector $\boldsymbol{u}_{fault}$ are given as

$$\boldsymbol{f}_1(\bar{\boldsymbol{x}}_1) = \begin{bmatrix} -2.1022n_h - 0.5281n_l + 12n_h^2 - n_l^2 \\ 1.9240n_h - 6.2069n_l - 1.7n_h^2 + n_l^2 \end{bmatrix}$$

$$B = \begin{bmatrix} 92.4704 & 7410.8640 \times 10^{-4} \\ 109.2637 & 74540.8101 \times 10^{-4} \end{bmatrix}$$

$$\boldsymbol{\alpha} = \begin{bmatrix} 5 & 0 \\ 0 & \frac{10}{3} \end{bmatrix}, \boldsymbol{\eta} = \begin{bmatrix} 0.1n_h \sin(n_l) \\ -0.1n_l \cos(n_h) \end{bmatrix}$$

$$\boldsymbol{u}_{fault} = \begin{cases} [0, 0]^{\mathrm{T}}, t < 10 \\ [0.5, 0.8]^{\mathrm{T}}, t \geq 10 \end{cases}$$

Suppose the initial deviation state vector from operating point is $\boldsymbol{x}(0) = [0.1, -0.1]^{\mathrm{T}}$.

In order to make comparison, simulations under the presented ADP-based ISMFTC method and the traditional sliding mode fault-tolerant control method (TradSMFTC) are illustrated in the following.

- **ADP-based ISMFTC method**

To choose Q and R in (10) as $Q = I_3$ and $R = 10 \times I_3$, where I_3 is three-dimensional identity matrix, and a critic NN is constructed to approximate the OCF (16) as

$$\hat{J}^*(\boldsymbol{x}_1) = W_{c1}n_h^2 + W_{c2}n_l^2 + W_{c3}n_h n_l$$

where $\boldsymbol{\sigma}_c = [n_h^2, n_l^2, n_h n_l]^{\mathrm{T}}$ is activation function and $\hat{\boldsymbol{W}}_c = [\hat{W}_{c1}, \hat{W}_{c2}, \hat{W}_{c3}]^{\mathrm{T}}$ is the estimation of the ideal weight of NN, respectively. Select the parameters α_c and α_s in (34) as $\alpha_c = 0.1, \alpha_s = 0.5$. Figure 5 shows that the evolution of the weight vector $\hat{\boldsymbol{W}}_c$, and the weight vector ultimately converges to $[0.0578, 0.0855, 0.0701]^{\mathrm{T}}$ finally.

According to the constant weight vector $\hat{\mathbf{W}}_c$, the novel ADP-based sliding surface (11) will be obtained.

To get satisfying controller parameters, $\dot{\hat{u}}_{fault} = 0$ GWO is applied to optimise $\boldsymbol{K}_s = \mathtt{diag}\{K_{s_1}, K_{s_2}\}$, $\boldsymbol{K}_f = \mathtt{diag}\{K_{f_1}, K_{f_2}\}$, therefore, it is suitable to let $\vec{X} = \left[K_{s_1}, K_{s_2}, K_{f_1}, K_{f_2}\right]$. Table 1 gives the parameters optimisation results based on GWO.

Simulation results under ADP-based ISMFTC method are given in 6 and Fig. 10.

https://doi.org/10.1017/aer.2024.68 Published online by Cambridge University Press

Table 1. *Parameters optimisation results based on GWO*

Parameters	Range	Results
K_{s_1}	0–10	2.3468
K_{s_2}	0–10	1.2236
K_{f_1}	0–20	9.8567
K_{f_2}	0–20	12.9465

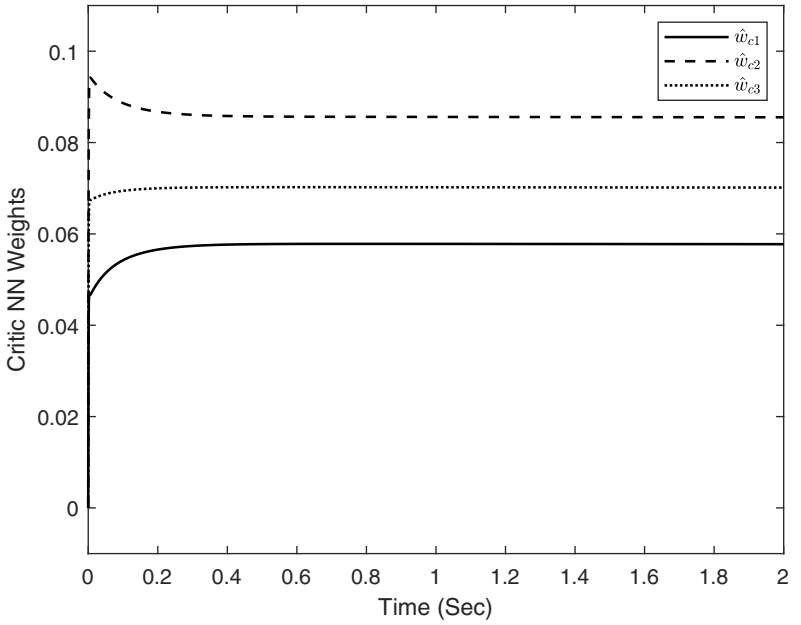


Figure 5. *Evolution of the critic NN weights* $\hat{\boldsymbol{W}}_c$.

- **TradSMFTC method**

Through the boundary layer technology, the classical SMC-based FTC is designed as

$$\boldsymbol{u}_0 = \boldsymbol{g}_2(\bar{\boldsymbol{x}})^{-1}\left(-\boldsymbol{f}_2(\bar{\boldsymbol{x}}) - \boldsymbol{g}_2(\bar{\boldsymbol{x}})\hat{\boldsymbol{u}}_{fault} - \boldsymbol{K}_f\left(\boldsymbol{f}_1(\bar{\boldsymbol{x}}_1) + \boldsymbol{g}_1(\bar{\boldsymbol{x}}_1)\bar{\boldsymbol{x}}_2\right) - \boldsymbol{K}_s\mathrm{sat}(\boldsymbol{s}_{trad})\right) \tag{43}$$

and the adaptive fault estimation is

$$\dot{\hat{\boldsymbol{u}}}_{fault} = \boldsymbol{K}_f\boldsymbol{g}_2(\bar{\boldsymbol{x}})\boldsymbol{s}_{trad} \tag{44}$$

where the sliding surface is $\boldsymbol{s}_{trad} = \dot{\bar{\boldsymbol{x}}}_1 + \boldsymbol{c}_{trad}\bar{\boldsymbol{x}}_1$ with $\mathbf{c}_{trad} = 0.1 \times I_2$, where I_2 is two-dimensional identity matrix. Let $\boldsymbol{K}_s$ and $\boldsymbol{K}_f$ are the same as those of in ADP-based ISMFTC method. The simulation results are given Figs. 11 and 12.

From Figs. 6–8, it can be found that fault estimation law (15) designed in this paper, can realise to estimate large abrupt actuator faults precisely in four seconds. By comparing Fig. 9 with Fig. 11, it is easy to see that the influence of both the initial deviations and the actuator faults, are much smaller under ADP-based ISMFTC method than those of under TradSMFTC method, including fluctuation, convergence and peak values. Figure 10 shows that the control signals are smoother than those of in Fig. 12, especially the signal of u_{0_2}. Tables 2 and 3 also illustrates this situation by comparing the root mean square. Therefore, the proposed ADP-based ISMFTC method has excellent performance.

https://doi.org/10.1017/aer.2024.68 Published online by Cambridge University Press

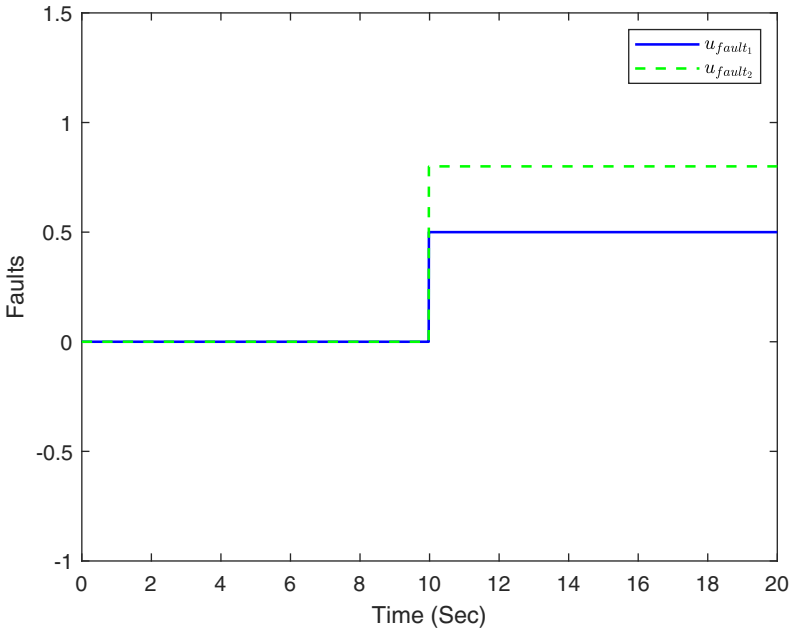


Figure 6. *Actuator faults in aircraft engine system.*

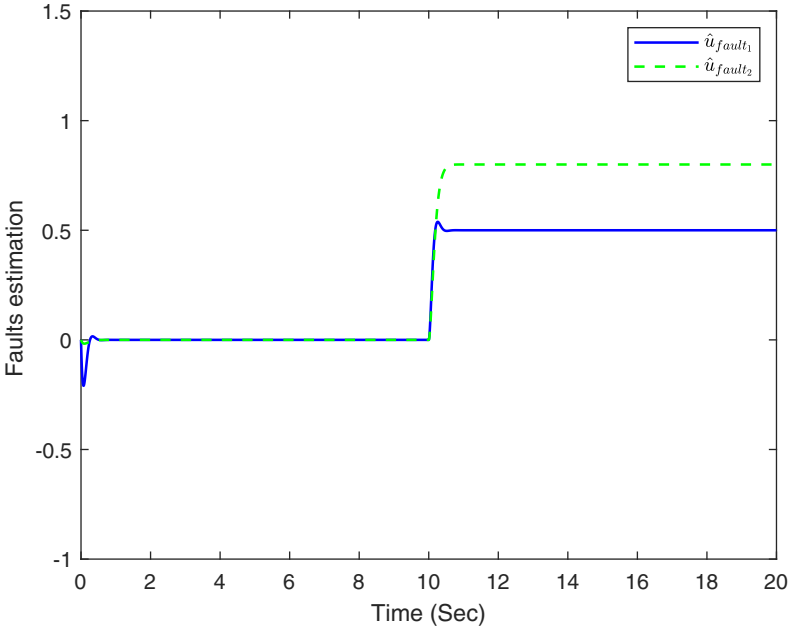


Figure 7. *Actuator faults estimation.*

5.0 Conclusions

An ADP-based intelligent sliding mode fault-tolerant control (ADP-based ISMFTC) method is proposed for aircraft engine systems with actuator dynamics and faults to ensure satisfying steady-state and dynamic performance, along with strong fault-tolerance performance.

https://doi.org/10.1017/aer.2024.68 Published online by Cambridge University Press

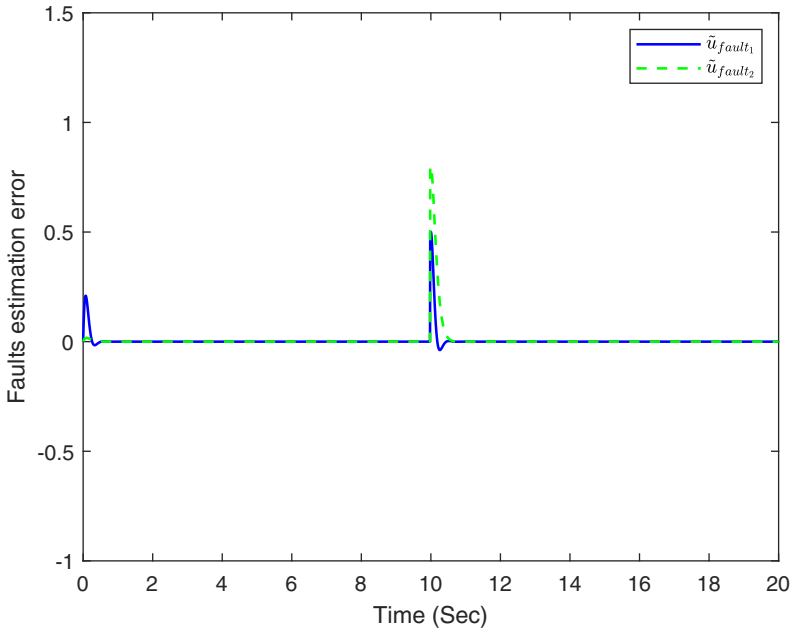


Figure 8. *Actuator faults estimation error.*

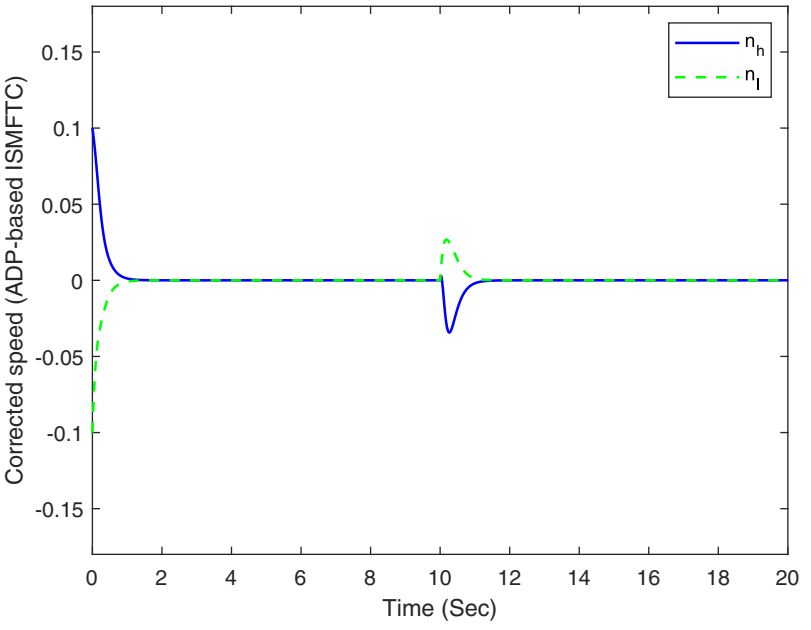


Figure 9. *Control results under ADP-based ISMFTC-n.*

The main characteristic of the ADP-based ISMFTC method are summarised as follows:

- On the basis of the features of aircraft engines and their actuators, an uncertain nonlinear cascaded model of aircraft engines with both actuator dynamics and actuator faults is formed.
- The presented sliding surface deals with mismatched uncertainty by ADP strategy, which can can suppress chattering, and can be solved by ADP strategy off-line.

https://doi.org/10.1017/aer.2024.68 Published online by Cambridge University Press

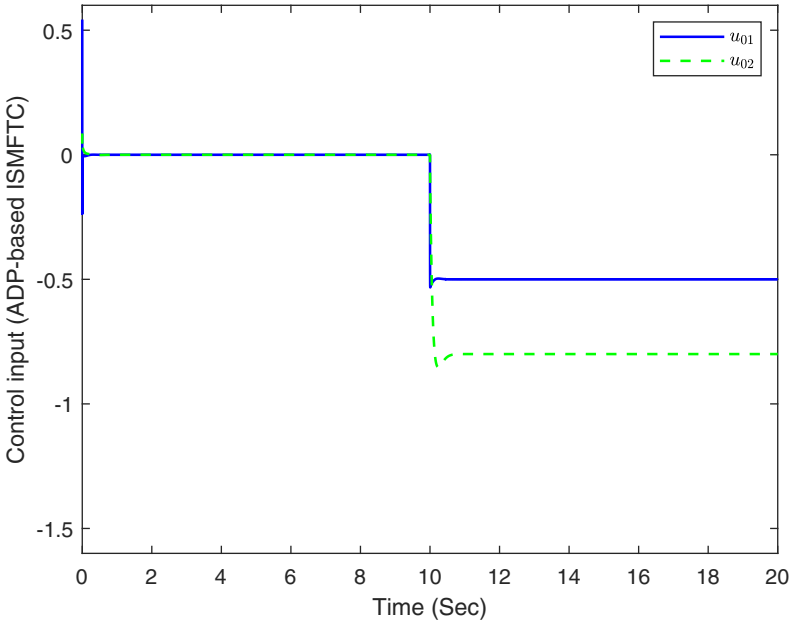


Figure 10. *Control results under ADP-based ISMFTC-u_0.*

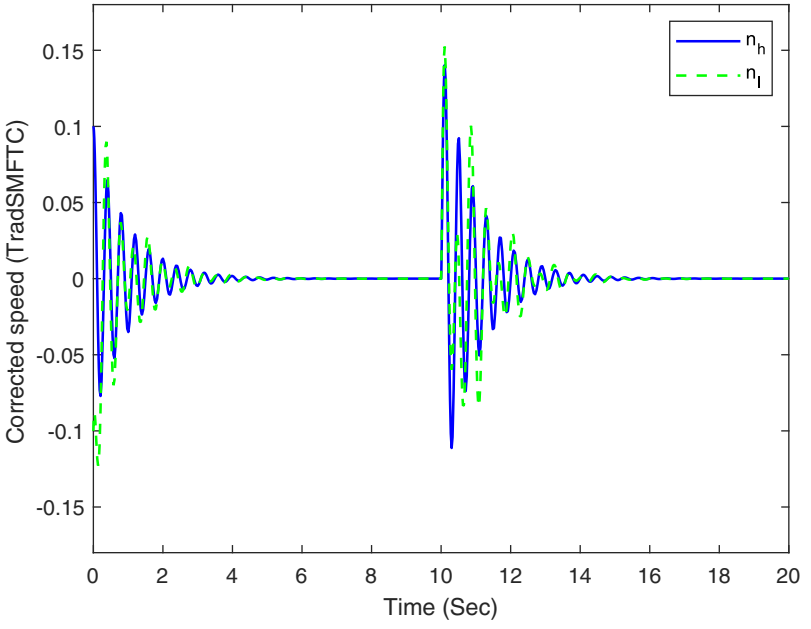


Figure 11. *Control results under TradSMFTC-n.*

- In order to get optimised designable control parameters, GWO is combined into the creation of the ADP-based ISMFTC method.
- Robustness analysis is given based on Lyapunov theory, the closed-loop system states is UUB and its fault estimation error is bounded at the same time.

https://doi.org/10.1017/aer.2024.68 Published online by Cambridge University Press

Table 2. *Root mean square-n comparison*

Method	n_h(0–10s)	n_l(0–10s)	n_h(10–20s)	n_l(10–20s)
TradSMFTC	0.01545	0.02091	0.02398	0.02471
ISMFTC	0.01276	0.00974	0.01375	0.00980

Table 3. *Root mean square-u_0 comparison*

Method	u_{01}(0–10s)	u_{02}(0–10s)	u_{01}(10–20s)	u_{02}(10–20s)
TradSMFTC	0.00881	0.07617	0.5003	0.8105
ISMFTC	0.00617	0.00800	0.5001	0.8083

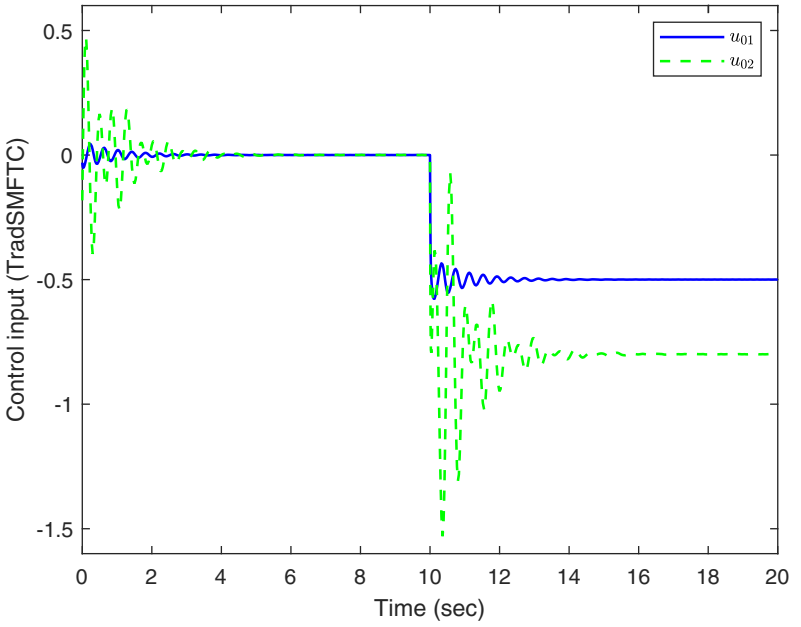


Figure 12. *Control results under TradSMFTC-u_0.*

Simulation results indicate that the proposed ADP-based ISMFTC method can make certain that the twin-shaft turbofan aircraft engine system has excellent performance, including high steady-state accuracy, smooth dynamic performance and strong fault tolerance and so on.

Acknowledgements. The authors would like to thank all of their lab-mates. This work is partially supported by High Performance Computing Platform of Nanjing University of Aeronautics and Astronautics.

References

[1] Richter, H. *Advanced Control of Turbofan Engines*, Springer Science & Business Media, 2011, New York.
[2] Zhu, P., Jiang, J. and Yu, C. Fault-tolerant control of hypersonic vehicles based on fast fault observer under actuator gain loss fault or stuck fault, *Aeronaut. J.*, 2020, **124**, (1278), pp 1190–1207.
[3] Xiao, L. and Lin, C. *Fault Diagnosis and Fault Tolerant Control of Aerospace Power Systems based on Sliding Mode Theory*, Beijing University of Aeronautics and Astronautics Press, 2022, Beijing, China.
[4] David Young, K., Utkin, V.I. and Ozguner, U. A control engineer's guide to sliding mode control, *IEEE Trans. Control Syst. Technol.*, 1999, **7,** (3), pp 328–342.
[5] Alwi, H., Edwards, C. and Tan, C.P. *Fault Detection and Fault-Tolerant Control Using Sliding Modes*, Springer, 2011, London.

https://doi.org/10.1017/aer.2024.68 Published online by Cambridge University Press

[6] Shtessel, Y., Edwards, C., Fridman, L., Levant, A., et al. *Sliding Mode Control and Observation*, vol. 10, Springer, 2014, New York.

[7] Zhang, K., Jiang, B., Yan, X., Mao, Z. and Polycarpou, M.M. Fault-tolerant control for systems with unmatched actuator faults and disturbances, *IEEE Trans. Autom. Control*, 2020, **66**, (4), pp 1725–1732.

[8] Shao, K., Zheng, J., Wang, H., Xu, F., Wang, X. and Liang, B. Recursive sliding mode control with adaptive disturbance observer for a linear motor positioned, *Mech. Syst. Signal Process.*, 2021, **146**, 107014.

[9] Zhang, Y., Shou, Y., Zhang, P. and Han, W. Sliding mode based fault-tolerant control of hypersonic reentry vehicle using composite learning, *Neurocomputing*, 2022, **484**, pp 142–148.

[10] Hou, S., Wang, C., Chu, Y. and Fei, J. Neural-observer-based terminal sliding mode control: Design and application, *IEEE Trans. Fuzzy Syst.*, 2022, **30**, (11), pp 4800–4814.

[11] Yang, J., Li, S. and Yu, X. Sliding-mode control for systems with mismatched uncertainties via a disturbance observer, *IEEE Trans. Ind. Electron.*, 2013, **60**, (1), pp 160–169.

[12] Riaz, U., Tayyeb, M. and Amin, A.A. A review of sliding mode control with the perspective of utilization in fault tolerant control, *Recent Adv. Electr. Electron. Eng. (Formerly Recent Patents on Electrical & Electronic Engineering)*, 2021, **14**, (3), pp 312–324.

[13] Yang, J., Li, S. and Yu, X. Sliding-mode control for systems with mismatched uncertainties via a disturbance observer, *IEEE Trans. Ind. Electron.*, 2012, **60**, (1), pp 160–169.

[14] Zhang, H., Qu, Q., Xiao, G. and Cui, Y. Optimal guaranteed cost sliding mode control for constrained-input nonlinear systems with matched and unmatched disturbances, *IEEE Trans. Neural Netw. Learn. Syst.*, 2018, **29**, (6), pp 2112–2126.

[15] Saeedi, M., Zarei, J., Razavi-Far, R. and Saif, M. Event-triggered adaptive optimal fast terminal sliding mode control under denial-of-service attacks, *IEEE Syst. J.*, 2021, **16**, (2), pp 2684–2692.

[16] Perrusqua, A., Flores-Campos, J.A. and Yu, W. Optimal sliding mode control for cutting tasks of quick-return mechanisms, *ISA Trans.*, 2021, **122**, pp 88–95.

[17] Richter, H. A multi-regulator sliding mode control strategy for output-constrained systems, *Automatica*, 2011, **47**, (10), pp 2251–2259.

[18] Shubo, Y., Xi, W. and Bei, Y. Adaptive sliding mode control for limit protection of aircraft engines, *Chin. J. Aeronaut.*, 2018, **31**, (7), pp 1480–1488.

[19] Yang, S.-B., Wang, X., Wang, H.-N. and Li, Y.-G. Sliding mode control with system constraints for aircraft engines, *ISA Trans.*, 2020, **98**, pp 1–10.

[20] Xiao, L., Du, Y., Hu, J. and Jiang, B. Sliding mode fault tolerant control with adaptive diagnosis for aircraft engines, *Int. J. Turbo Jet-Engines*, 2018, **35**, (1), pp 49–57.

[21] Xiao, L., Sattarov, R.R., Liu, P. and Lin, C. Intelligent fault-tolerant control for AC/DC hybrid power system of more electric aircraft, *Aerospace*, 2022, **9**, (1), 4.

[22] Li, W., Wen, Q. and Zhou, H. Adaptive sliding mode formation control for multiple flight vehicles with considering autopilot dynamic, *Aeronaut. J.*, 2021, **125**, (1290), pp 1337–1357.

[23] Wang, D., Liu, D., Li, H. and Ma, H. Neural-network-based robust optimal control design for a class of uncertain nonlinear systems via adaptive dynamic programming, *Inform. Sci.*, 2014, **282**, pp 167–179.

[24] Fan, Q.Y. and Yang, G.H. Adaptive actor–critic design-based integral sliding-mode control for partially unknown nonlinear systems with input disturbances, *IEEE Trans. Neural Netw. Learn. Syst.*, 2015, **27,** (1), pp 165–177.

[25] Du, Y., Jiang, B., Ma, Y. and Cheng, Y. Robust adp-based sliding-mode fault-tolerant control for nonlinear systems with application to spacecraft, *Appl. Sci.*, 2022, **12**, (3), p 1673.

[26] Mirjalili, S., Mohammad Mirjalili, S. and Lewis, A. Grey wolf optimizer, *Adv. Eng. Software*, 2014, **69**, pp 46–61.

[27] Faris, H., Aljarah, I., Azmi Al-Betar, M. and Mirjalili, S. Grey wolf optimizer: a review of recent variants and applications, *Neural Comput. Appl.*, 2018, **30**, (2), pp 413–435.

[28] Sharma, I., Kumar, V. and Sharma, S. A comprehensive survey on grey wolf optimization, *Recent Adv. Comput. Sci. Commun. (Formerly: Recent Patents on Computer Science)*, 2022, **15**, (3), pp 323–333.

[29] Yu, D., Liu, X., Bao, W. and Xu, Z. Multiobjective robust regulating and protecting control for aeroengines, *J. Eng. Gas Turbines Power*, 2009, **131**, (6), pp 061601.

[30] Wang, J., Ye, Z. and Hu, Z. Nonlinear control of aircraft engines using a generalized gronwall-bellman lemma approach, *J. Eng. Gas Turbines Power*, 2012, **134**, (9), p 094502 1–6.

[31] Xiao, L. and Ye, Z. *Optimal Control for Aerospace Power System*, Beijing University of Aeronautics and Astronautics Press, 2021, Beijing, China.

[32] Krstic, M., Kokotovic, P.V. and Kanellakopoulos, I. Nonlinear and adaptive control design, *Lecture Notes in Control & Information Sciences*, 1995, **5**, (2), pp 4475–4480.

[33] Wang, Z., Liu, X., Liu, K., Li, S. and Wang, H. Backstepping-based lyapunov function construction using approximate dynamic programming and sum of square techniques, *IEEE Trans. Cybern.*, 2016, **47**, (10), pp 3393–3403.

[34] Jiang, B., Staroswiecki, M. and Cocquempot, V. Fault accommodation for nonlinear dynamic systems, *IEEE Trans. Autom. Control*, 2006, **51**, (9), pp 1578–1583.

[35] Zhang, K., Jiang, B. and Cocquempot, V. Adaptive observer-based fast fault estimation, *Int. J. Control Autom. Syst.*, 2008, **6**, (3), pp 320–326.

[36] Tang, G.-Y., Dong, R. and Gao, H.-W. Optimal sliding mode control for nonlinear systems with time-delay, *Nonlinear Anal.-Hybrid Syst.*, 2008, **2**, (3), pp 891–899.

[37] Huang, J., Zhang, T., Ye, Z., Zhou, W. and Pan, M. *Modern Aviation Power Plant Control*, *3rd ed*, Aviation Industry Press, 2018, Beijing, China.

https://doi.org/10.1017/aer.2024.68 Published online by Cambridge University Press

[38] Gao, W. *Variable Structure Control Theory and Design Method*, Science Publishing House, 1996, Beijing, China.
[39] Abu-Khalaf, M. and Lewis, F.L. Nearly optimal control laws for nonlinear systems with saturating actuators using a neural network hjb approach, *Automatica*, 2005, **41**, (5), pp 779–791.
[40] Wang, D., Liu, D., Mu, C. and Zhang, Y. Neural network learning and robust stabilization of nonlinear systems with dynamic uncertainties, *IEEE Trans. Neural Netw. Learn. Syst.*, 2017, **29**, (4), pp 1342–1351.
[41] Vamvoudakis, K.G. and Lewis, F.L. Online actor–critic algorithm to solve the continuous-time infinite horizon optimal control problem, *Automatica*, 2010, **46**, (5), pp 878–888.
[42] Wang, D., Liu, D., Zhang, Y. and Li, H. Neural network robust tracking control with adaptive critic framework for uncertain nonlinear systems, *Neural Netw.*, 2018, **97**, pp 11–18.
[43] Du, Y., Jiang, B. and Ma, Y. Policy iteration based online adaptive optimal fault compensation control for spacecraft, *Int. J. Control Autom. Syst.*, 2021, **19**, (4), pp 1607–1617.
[44] Mirjalili, S., Mohammad Mirjalili, S. and Lewis, A. Grey wolf optimizer, *Adv. Eng. Software*, 2014, **69**, pp 46–61.

Cite this article: Xiao L.F., Tan Y.S., Du Y.B and Zhang X.L (2025). Intelligent sliding mode fault-tolerant control for aircraft engines with actuator dynamics and faults based on adaptive dynamic programming. *The Aeronautical Journal*, **129**, 651–670. https://doi.org/10.1017/aer.2024.68

https://doi.org/10.1017/aer.2024.68 Published online by Cambridge University Press